Relationship between meteoric ^{10}Be and NO$_3^-$ concentrations in soils along the Shackleton Glacier, Antarctica

Melisa A. Diaz[1,2†], Lee B. Corbett[3], Paul R. Bierman[3], Byron J. Adams[4], Diana H. Wall[5], Ian D. Hogg[6,7], Noah Fierer[8], W. Berry Lyons[1,2]

[1]School of Earth Sciences, The Ohio State University, Columbus, OH, 43210, USA
[2]Byrd Polar and Climate Research Center, The Ohio State University, Columbus, OH, 43210, USA
[3]Department of Geology, University of Vermont, Burlington, VT, 05405, USA
[4]Department of Biology, Evolutionary Ecology Laboratories, and Monte L. Bean Museum, Brigham Young University, Provo, UT, 84602, USA
[5]Department of Biology and School of Global Environmental Sustainability, Colorado State University, Fort Collins, CO, 80523, USA
[6]Canadian High Arctic Research Station, Polar Knowledge Canada, Cambridge Bay, NU, X0B0C0, Canada
[7]School of Science, University of Waikato, Hamilton, 3216, New Zealand
[8]Department of Ecology and Evolutionary Biology and Cooperative Institute for Research in Environmental Science, University of Colorado Boulder, Boulder, CO, 80309, USA
[†]Now at Departments of Geology and Geophysics, and Applied Ocean Physics and Engineering, Woods Hole Oceanographic Institution, Woods Hole, MA, 02543, USA

Correspondence to: Melisa A. Diaz (mdiaz@whoi.edu)

Abstract. Outlet glaciers that flow through the Transantarctic Mountains (TAM) experienced changes in ice thickness greater than other coastal regions of Antarctica during glacial maxima. As a result, ice-free areas that are currently exposed may have been covered by ice at various points during the Cenozoic, complicating our understanding of ecological succession in TAM soils. Our knowledge of glacial extent on small spatial scales is limited for the TAM, and studies of soil exposure duration and disturbance, in particular, are rare. We collected surface soil samples, and in some places, depth profiles every 5 cm to refusal (up to 30 cm) from eleven ice-free areas along the Shackleton Glacier, a major outlet glacier of the East Antarctic Ice Sheet. We explored the relationship between meteoric ^{10}Be and NO$_3^-$ in these soils as a tool for understanding landscape disturbance and wetting history, and as exposure proxies. Concentrations of meteoric ^{10}Be spanned more than an order of magnitude across the region (2.9 x 10^8 atoms g^{-1} to 73 x 10^8 atoms g^{-1}) and are among the highest measured in polar regions. The concentrations of NO$_3^-$ were similarly variable and ranged from ~1 µg g^{-1} to 15 mg g^{-1}. In examining differences and similarities in the concentrations of ^{10}Be and NO$_3^-$ with depth, we suggest that much of the southern portion of the Shackleton Glacier region has likely developed under a hyper-arid climate regime with minimal disturbance. Finally, we inferred exposure time using ^{10}Be concentrations. This analysis suggests that the soils we analyzed likely range from recent exposure (following the Last Glacial Maximum) to possibly >6 Ma. Our data suggest that further testing and interrogation of meteoric ^{10}Be and NO$_3^-$ concentrations and relationships in soils can provide important information regarding landscape development, soil evolution processes, and inferred exposure durations of surfaces in the TAM.

1

1. Introduction

One of the most intriguing questions in biogeography concerns the relationship between the evolution of terrestrial organisms and landscape disturbance (e.g., glacial overriding, soil wetting), particularly in Antarctica. Current data indicate that organism lineages have survived in some Antarctic soils for possibly millions of years, despite multiple glaciations throughout the Pleistocene (Convey et al., 2008; Fraser et al., 2012; Stevens and Hogg, 2003). It is still unclear how and where these organisms found suitable glacial refugia given the high salt concentrations in high-elevation soils (Lyons et al., 2016). The most biodiverse soils in the Ross Sea sector are at low elevations near the coast, where the Ross Ice Shelf or sea ice meet the Transantarctic Mountains (TAM) (Collins et al., 2020). These soils are also those which are most susceptible to glacial overriding during glacial maxima, though the timing of retreat and glacial extent is still unknown on local scales (Golledge et al., 2012; Mackintosh et al., 2011).

Outlet glaciers are among the most sensitive areas to glaciological change in Antarctica, and changes in their extents over time are recorded in nearby sedimentary deposits (Golledge et al., 2013; Jones et al., 2015; Scherer et al., 2016; Spector et al., 2017). However, only scattered information exits on TAM soil processes, ages and chronosequences, and the implications for terrestrial and ecosystem history (Bockheim, 2002; Dickinson et al., 2012; Graham et al., 2002, 1997; Lyons et al., 2016; Scarrow et al., 2014; Schiller et al., 2009). The Shackleton Glacier, an outlet glacier of the East Antarctic Ice Sheet (EAIS), flows between several exposed peaks of the Central Transantarctic Mountains (CTAM) and ice-free areas are present at both low and high elevations. We report concentrations of meteoric ^{10}Be and nitrate (NO_3^-) in soils from eleven distinct ice-free areas and investigate their distributions at depth to explore ^{10}Be and NO_3^- relationships. The sampling methodology was designed to capture a range of soils which have low salt concentrations due to recent exposure from glacial retreat following the Last Glacial Maximum (LGM) and soils that were likely exposed since at least the last glacial period. These data include some of the only meteoric ^{10}Be and NO_3^- concentration data from the CTAM (Claridge and Campbell, 1968b, 1977; Graham et al., 1997; Lyons et al., 2016), inform knowledge of landscape disturbance and wetting history, may potentially be used to infer soil exposure duration, and are useful in understanding Antarctic terrestrial biogeography.

2. Background

2.1. Brief overview of Antarctic glacial and wetting history

Antarctica is believed to have maintained a persistent ice sheet since at least the Eocene epoch, and the East and West Antarctic Ice Sheets (EAIS and WAIS, respectively) have waxed and waned since at least the Miocene (Gasson et al., 2016; Gulick et al., 2017). Sediment core records collected from the Ross Sea and ice cores from the Antarctic interior indicate that the EAIS and WAIS have undergone dozens of glacial and interglacial cycles throughout the Cenozoic (Augustin et al., 2004; Talarico et al., 2012). The WAIS is a marine-terminating ice sheet with a grounding line below sea level, which decreases the stability of the ice sheet and results in rapid advance and retreat compared to the EAIS (Pollard and DeConto, 2009). The EAIS is grounded above sea level and is generally more stable. The EAIS and WAIS were at their most recent greatest extent about 14 ka during the LGM (Clark et al., 2009). During the LGM, the EAIS expanded along its margins and some of the greatest increases in height occurred at outlet glaciers which flow through exposed peaks of the TAM and drain into the Ross and Weddell Seas (Anderson et al., 2002; Golledge et al., 2012; Mackintosh et al., 2014). As a result, many of the currently exposed TAM soils were overrun by ice during the LGM and some may have only recently been exposed.

Much of the Antarctic continent is a polar desert and geomorphological data from ice-free soils in the McMurdo Dry Valleys indicate that some regions have likely been hyper-arid for as long as 15 Ma (Marchant et al., 1996; Valletta et al., 2015). As such, atmospherically-derived constituents, including salts and metals, can accumulate in exposed Antarctic soils at concentrations similar to those from the Atacama and Namib Deserts (Diaz et al., 2020; Lyons et al., 2016; Reich and Bao, 2018). Using soil NO_3^- concentrations from the Meyer Desert in the Beardmore Glacier region and NO_3^- fluxes calculated from a Dominion Range ice core, Lyons et al. (2016)

85   estimated that at least 750,000 years have passed since the Meyer Desert had wide-spread soil wetting. It is likely
86   that other high elevation and inland locations in the TAM also have high concentrations of salts and similarly old
87   "wetting ages", though this has not been thoroughly investigated.

2.2. Meteoric ^{10}Be systematics in Antarctic soils

89   ^{10}Be is a cosmogenic radionuclide with a half-life of 1.39 Ma (Korschinek et al., 2010) that is produced
90   both in the atmosphere (meteoric) and *in-situ* in mineral grains. In the atmosphere, N and O gases are bombarded by
91   high energy cosmic radiation to produce meteoric ^{10}Be. Particle reactive ^{10}BeO or ^{10}Be(OH)$_2$ is produced and
92   removed from the atmosphere by wet and dry deposition (McHargue and Damon, 1991). At Earth's surface,
93   meteoric ^{10}Be sorbs onto clay particles and is insoluble in most natural waters of pH greater than 4 (Brown et al.,
94   1992; You et al., 1989). The clay particles can be redistributed to lower depths in soils due to particle migration or
95   can be transported by winds. As such, the total number of ^{10}Be atoms in a soil profile, its inventory, is a function of
96   surface exposure duration, erosion, clay particle translocation, solubility, and sedimentation. If delivery rates can be
97   determined, meteoric ^{10}Be can be used as a tool to understand exposure ages, erosion rates, and soil residence times
98   (see Willenbring and Von Blanckenburg, 2009 and references within). There are scattered exposure age studies from
99   across the CTAM using a variety of *in-situ* produced cosmogenic nuclides (Ackert and Kurz, 2004; Balter-Kennedy
100 et al., 2020; Bromley et al., 2010; Kaplan et al., 2017; Spector et al., 2017), and previously reported exposure ages
101 of CTAM moraines and boulders from these studies ranged from <10 ka to >14 Ma.

102 The measurement of meteoric ^{10}Be in soil has enabled researchers to date surfaces (soils) and features in
103 Antarctica. Previous studies have measured meteoric ^{10}Be in the McMurdo Dry Valleys (MDV) and Victoria Land
104 soils and sediments to calculate exposure ages and to determine the onset of the current polar desert regime
105 (Dickinson et al., 2012; Graham et al., 2002; Schiller et al., 2009; Valletta et al., 2015). In general, these previous
106 studies found that high elevation, northern fringe regions along the Ross Embayment have been ice-free and
107 possibly hyper-arid since at least the Pliocene. Few meteoric ^{10}Be data have been previously published from the
108 CTAM (Graham et al., 1997), which represent ice sheet dynamics and climatic conditions closer to the Polar
109 Plateau.

2.3. Nitrate systematics in Antarctic soils

111 The nitrogen cycle in Antarctica differs greatly from the nitrogen cycle in temperate regions, primarily due
112 to scarce biomass and few vascular plants (Cary et al., 2010; Michalski et al., 2005). Nitrogen in CTAM soils
113 primarily exists as NO_3^- and is sourced from the atmosphere, with varying contributions from the troposphere and
114 stratosphere (Diaz et al., 2020; Lyons et al., 2016; Michalski et al., 2005). Similar to meteoric ^{10}Be, NO_3^- is
115 deposited on exposed soils, however, nitrate salts are highly water-soluble. Once deposited on the surface, nitrate
116 salts can be dissolved and transported down gradient or eluted to depth when wetted (i.e., during ice/snow melt
117 events). However, the hyper-arid climate of the CTAM can allow NO_3^- to accumulate at high concentrations in soils
118 (Claridge and Campbell, 1968a; Diaz et al., 2020; Lyons et al., 2016). Soil NO_3^- concentrations have the potential to
119 inform our knowledge of wetting history and possibly glacial history in the CTAM due to the relatively high
120 solubility of nitrate salts, though uncertainties regarding heterogeneous deposition and post-depositional alteration
121 (such as re-volatilization and photolysis) require further investigation (Diaz et al., 2020; Frey et al., 2009; Graham et
122 al., 2002).

3. Study sites and region

124 Shackleton Glacier (~84.5 to 86.4°S; ~130 km long and ~10 km wide) is a major outlet glacier of the EAIS
125 that drains north into the Ross Embayment with other CTAM outlet glaciers to form the Ross Ice Shelf (RIS) (Fig.
126 1). The ice flows between exposed surfaces of the Queen Maud Mountains, which range from elevations of ~150 m
127 near the RIS to >3,500 m further inland. The basement geology of the Shackleton Glacier region is comprised of
128 igneous and metamorphic rocks that formed from intruded and metamorphosed sedimentary and volcanic strata
129 during the Ross Orogeny (450-520 Ma) (Elliot and Fanning, 2008). The southern portion of the region consists of
130 the Devonian-Triassic Beacon Supergroup and the Jurassic Ferrar Group, while the northern portions consists of

Pre-Devonian granitoids and the Early to Mid-Cambrian Taylor Group (Elliot and Fanning, 2008; Paulsen et al., 2004). These rocks serve as primary parent material for soil forma (Claridge and Campbell, 1968b). Deposits of the Sirius Group, the center of the stable vs. dynamic EAIS debate, have been previously identified in the southern portion of the Shackleton Glacier region, particularly at Roberts Massif (Fig. 2) and Bennett Platform, with a small exposure at Schroeder Hill (Hambrey et al., 2003).

The valleys and other ice-free areas within the region have been modified by the advance and retreat of the Shackleton Glacier, smaller tributary glaciers, and alpine glaciers. Similar to the Beardmore Glacier region, the Shackleton Glacier region is a polar desert, which results in the high accumulation of salts in soils. The surface is comprised primarily of till, weathered primary bedrock, and scree, which ranges in size from small boulders and cobbles to sand and silt. Clay minerals have been previously identified in all samples from Roberts Massif and are likely ubiquitous throughout the region (Claridge and Campbell, 1968b). The clays are a mixture of those derived from sedimentary rocks and contemporaneous weathering (Claridge and Campbell, 1968b). Thin, boulder belt moraines, characteristic of cold-based glaciers, were deposited over bedrock and tills at Roberts Massif, while large moraines were deposited at Bennett Platform (Fig. 2; Balter-Kennedy et al., 2020; Claridge and Campbell, 1968). Most soils appeared dry, though some small ponds and water tracks have been documented near Mt. Heekin and Thanksgiving Valley (Elliot et al., 1996). Additional information on the sample locations and surface features is provided in Tables 1 and 2.

4. Methods

4.1. Sample collection

During the 2017-2018 austral summer, we visited eleven ice-free areas along the Shackleton Glacier: Roberts Massif, Schroeder Hill, Bennett Platform, Mt. Augustana, Mt. Heekin, Thanksgiving Valley, Taylor Nunatak, Mt. Franke, Mt. Wasko, Nilsen Peak, and Mt. Speed (Fig. 1). These areas represent soils from near the head of the glacier to near the glacier terminus at the coast of the RIS. Two surface samples (Table 1) were collected at each location (except for Nilsen Peak and Mt. Wasko, represented by only one sample each) with a plastic scoop and stored in Whirl-Pak™ bags. One sample was collected furthest from the Shackleton Glacier or other tributary glaciers (within ~2,000 m) to represent soils that were likely exposed during the LGM and previous recent glacial periods. A second sample was collected closer to the glacier (between ~1,500 and 200 m from the first sample) to represent soils likely to have been covered during the LGM and exposed by more recent ice margin retreat.

Soil pits were dug by hand at the sampling locations furthest from the glacier for Roberts Massif, Schroeder Hill, Mt. Augustana, Bennett Platform, Mt. Heekin, Thanksgiving Valley, and Mt. Franke (7 sites). Continuous samples were collected every 5 cm until refusal (up to 30 cm) and stored frozen in Whirl-Pak™ bags. All surface (21) and depth profile (25) samples were shipped frozen to The Ohio State University and kept frozen until analyzed. We selected Roberts Massif, Bennett Platform, and Thanksgiving Valley as locations for the most in-depth analysis for the depth profiles. These locations were chosen to maximize variability in landscape development: Roberts Massif represented an older, likely minimally disturbed landscape; Thanksgiving Valley represented a landscape with possible hydrologic activity, as evidenced by nearby ponds; Bennett Platform represented a landscape with evidence of recent glacial advance and retreat, and substantial topographic highs and lows (Table 2).

4.2. Analytical methods

4.2.1. Meteoric ^{10}Be analysis

A total of 30 sub-samples of surface soils from all locations, and the depth profiles from Roberts Massif, Bennett Platform, and Thanksgiving Valley, were sieved to determine the grain size at each location For each sample, the percentages of gravel (>2 mm), sand (63 µm-2 mm), and silt (<63 µm) are reported in Table S1. Since there is a strong grain size dependence of meteoric ^{10}Be (little ^{10}Be is carried on coarse (>2 mm) grains (Pavich et al., 1986)) the gravel portion of the sample was not included in the meteoric ^{10}Be analysis. The remaining soil (<2 mm) was ground to fine powder using a shatterbox.

4

177   Meteoric [10]Be (Table 1; S2) was extracted and purified at the NSF/University of Vermont (UVM)
178 Community Cosmogenic Facility following procedures adapted from Stone (1998). First, 0.5 g of powdered soil was
179 weighed into platinum crucibles and 0.4 g of SPEX [9]Be carrier (with a concentration of 1,000 μg mL^{-1}) was added to
180 each sample. The samples were fluxed with a mixture of potassium hydrogen fluoride and sodium sulfate. Perchloric
181 acid was then added to remove potassium by precipitation and later evaporated. Samples were dissolved in nitric
182 acid and precipitated as beryllium hydroxide (Be(OH)$_2$) gel, then packed into stainless steel cathodes for accelerator
183 mass spectrometer isotopic analysis at the Purdue Rare Isotope Measurement (PRIME) Laboratory. Isotopic ratios
184 were normalized to primary standard 07KNSTD with an assumed ratio of 2.85 x 10^{-12} (Nishiizumi et al., 2007). We
185 corrected sample ratios with a [10]Be/[9]Be blank ratio of 8.2 ± 1.9 x 10^{-15}, which is the average standard deviation of
186 two blanks processed alongside the samples. We subtracted the blank ratio from the sample ratios and propagated
187 uncertainties in quadrature. Blank correction is not significant.

4.2.2. NO$_3^-$ analysis

189   Separate, un-sieved sub-samples of soil from all locations and depth profiles were leached at a 1:5 soil to
190 DI water ratio for 24 hours, then filtered through a 0.4 µm Nuclepore membrane filter. The leachate was analyzed on
191 a Skalar San++ Automated Wet Chemistry Analyzer with an SA 1050 Random Access Auto-sampler (Lyons et al.,
192 2016; Welch et al., 2010). Concentrations are reported as NO$_3^-$ (Table 1) with accuracy, as determined using a
193 USGS 2015 "round-robin" standard, and precision better than 5% (Lyons et al., 2016).

4.3. Meteoric [10]Be inventory

195   We developed a mass balance using the fluxes of meteoric [10]Be to and from Shackleton Glacier region soils
196 to understand the accumulation of [10]Be in glaciated environments (Pavich et al., 1984, 1986). The model assumes
197 that soils that were overlain by glacial ice in the past and are now exposed, accumulated less [10]Be than soils that
198 were exposed throughout the glacial periods (Fig. 3). The concentration of meteoric [10]Be at the surface (N, atoms g^{-1})
199 per unit of time (dt) is expressed as a function, where the addition of [10]Be is represented as the atmospheric flux to
200 the surface (Q, atoms cm^{-2} yr^{-1}), and removal is due to both radioactive decay, which is represented by a
201 disintegration constant (λ, yr^{-1}), and erosion (E, cm yr^{-1}) (Eq. 1). Particle mobility into the soil column is represented
202 by a diffusion constant (D, cm^2 yr^{-1}). The differential in depth is represented by dz.

203    $$\frac{dN}{dt} = Q - \lambda N - E\frac{dN}{dz} - D\frac{d^2N}{dz^2} \tag{1}$$

204   We accounted for uncertainties regarding [10]Be migration in the soil column by calculating the inventory (I,
205 atoms cm^{-2}) of the soil (Eq. 2) (Pavich et al., 1986). We used a density (ρ) of 2 g cm^{-3} and assumed that Q had not
206 changed systematically over the accumulation interval. The inventory is the total sum of meteoric [10]Be atoms in the
207 soil profile and the change in inventory due to deposition, decay, and surface erosion is related surface exposure
208 duration (Eq. 3).

209    $$I = \sum N \cdot \rho \cdot dz \tag{2}$$

210    $$\frac{dI}{dt} = Q - \lambda I - EN \tag{3}$$

211   Meteoric [10]Be concentrations typically decrease with depth until they reach a "background" level (Graly et
212 al., 2010). The background is identified as the point where the concentration of meteoric [10]Be is constant with depth
213 ($\frac{dN}{dz} = 0$). Typically, the background values can be used to calculate an initial inventory (I_i, atoms cm^{-2}) using Eq. 4,
214 where N_z is the [10]Be concentration (atoms g^{-1}) at the bottom of the profile (z, cm). In this case, we assume that the
215 initial concentration of meteoric [10]Be is isotropic. However, an accurate initial inventory can only be determined for
216 soil profiles that are deep enough to capture background concentrations. This may not be the case in areas of
217 permafrost where [10]Be is restricted to the active layer (Bierman et al., 2014).

218    $$I_i = N_z \cdot \rho \cdot z \tag{4}$$

219   Additionally, the initial inventory can be influenced by repeated glacier advance and retreat during glacial-
220   interglacial cycles. For this case, the soil has "inherited" ^{10}Be during each subsequent exposure to the atmosphere,
221   some of which may have been removed with eroded soil (Fig. 3c-d). For constructional landforms, such as moraines,
222   the inheritance is equal to the background/initial inventory. Without information on drift sequences, it is difficult to
223   correct the measured inventory for inheritance by distinguishing meteoric ^{10}Be that was deposited after the most
224   recent ice retreat from ^{10}Be that was deposited during previous interglacial periods.

225   **5. Results**
226   **5.1. Depth profile composition and concentrations of meteoric ^{10}Be**
227   Sediment grain size is similar among the three soil profiles collected from Roberts Massif, Bennett
228   Platform, and Thanksgiving Valley; the soils are primarily comprised of sand-sized particles, with less silt-sized and
229   smaller material (Fig. 4). The proportions of silt and gravel are similar at Roberts Massif, although the majority of
230   the profile is sand-sized. Thanksgiving Valley has the coarsest material, while Bennett Platform has a more even
231   grain size distribution. The deepest profile is from Thanksgiving Valley, while the Roberts Massif and Bennett
232   Platform profiles are half the depth. All three profiles are ice-cemented at the bottom and are shallow compared
233   those collected from the McMurdo Dry Valleys (Dickinson et al., 2012; Schiller et al., 2009; Valletta et al., 2015),
234   though they are comparable to profiles collected at Roberts Massif by Graham et al. (1997).

235   Concentrations of meteoric ^{10}Be for both surface and depth profiles samples span more than an order of
236   magnitude in the Shackleton Glacier region and range from 2.9×10^8 atoms g^{-1} at Mount Speed to 73×10^8 atoms g^{-1}
237   at Roberts Massif (Fig. 5; Table 1). At individual sites where samples were collected at two locations,
238   concentrations are typically highest for the samples furthest from the glacier, with notable exceptions at Roberts
239   Massif and Thanksgiving Valley (Fig. 5). This trend is expected since our sampling plan was designed to capture
240   both recently exposed soils (near the glacier(s)) and soils which have been exposed throughout the LGM and
241   possibly other glacial periods. The measured inventories (Eq. 2) vary from 0.57×10^{11} atoms at Bennett Platform to
242   1.5×10^{11} atoms at Roberts Massif (Table 3).

243   The meteoric ^{10}Be depth profiles differ between Roberts Massif, Bennett Platform, and Thanksgiving
244   Valley. The profile from Roberts Massif has the highest overall concentrations (Fig. 6). Within the profile, the 5-10
245   cm sampling interval has the highest concentration, followed by the bottom of the profile, then the surface. The
246   profile behavior for Thanksgiving Valley is similar, though the differences in concentrations within both profiles are
247   relatively small. Bennett Platform is the only location where the surface concentration is the highest compared to the
248   remainder of the profile and the concentration decreases with depth (Fig. 6). Although we sampled the entirety of
249   the active layer where modern particle mobility throughout the soil column occurs, no depth profiles appear to
250   decrease to background levels needed to calculate an initial meteoric ^{10}Be inventory (Eq. 4). As a result, we are not
251   able to correct the measured inventory for background ^{10}Be, nor are we able estimate the inherited ^{10}Be
252   concentration in the soil.

253   **5.2. Variability of NO_3^-**
254   Measured concentrations of NO_3^- span four orders of magnitude across the seven depth profiles we sampled
255   (Fig. 6; Table 1). The lowest concentration is from Mt. Franke, ~1 µg g^{-1}; the highest concentration is from Roberts
256   Massif, 15 mg g^{-1}. In addition, similar to the meteoric ^{10}Be profiles, the NO_3^- concentrations are highest for the
257   samples that were collected furthest from the coast and at the highest elevations (Table 1). In general, the profiles
258   from Roberts Massif and Thanksgiving Valley are similar (Fig. 6b); ^{10}Be and NO_3^- concentrations are highest just
259   below the surface in the 5-10 cm interval and are fairly consistent throughout the profile. The NO_3^- depth profile
260   mirrors the ^{10}Be profile at Bennett Platform – while ^{10}Be concentration decreases with depth, the NO_3^- concentration
261   increases with depth.

262   Since we measured NO_3^- concentrations for all seven depth profiles we collected, we compare the profile
263   concentrations and shapes from the four profiles without ^{10}Be depth measurements (Mt. Augustana, Schroeder Hill,

264 Mt. Franke, and Mt. Heekin) to the Roberts Massif, Bennett Platform, and Thanksgiving Valley profiles with both
265 measurements (Fig. 6). Most of the NO_3^- profiles do not significantly change with depth and are similar to the
266 profile from Thanksgiving Valley, though Schroeder Hill is most similar to Roberts Massif (Fig. 6). This is
267 unsurprising given the similar latitudes, surface features, and environmental conditions between the different
268 locations (e.g., high latitude hyper-arid vs. lower latitude with possible evidence of wetter conditions) (Fig. 1; Table
269 2). No other location had large terminal moraines, as observed at Bennett Platform.

6. Discussion

271 The Shackleton Glacier region soil profiles and surface samples are among the highest meteoric ^{10}Be
272 concentrations (~10^9 atoms g^{-1}) yet measured in Earth's polar regions (Fig. 6a). Though our profiles are shallower
273 than profiles from the MDV and Victoria Land in Antarctica (Dickinson et al., 2012; Schiller et al., 2009; Valletta et
274 al., 2015) and Sweden and Alaska in the Arctic (Bierman et al., 2014; Ebert et al., 2012), the soils from these
275 previous studies reached background concentrations of ^{10}Be within the top 40 cm, which is close to our maximum
276 depth of 30 cm at Thanksgiving Valley. For comparison, the deepest profile collected by Graham et al. (1997) at
277 Roberts Massif was 36 cm. The Bennett Platform soil profile is most similar to the soil profiles from other regions in
278 Antarctica, as they have decreasing ^{10}Be concentrations with depth, while Thanksgiving Valley and Roberts Massif
279 are relatively homogenous and more similar to profiles from the Arctic.

280 The inventories from this study are also among the highest calculated for Antarctic soils. The inventories
281 from Bennett Platform and Thanksgiving Valley are most similar (~10^{10}) to inventories of saprolites and tills from
282 Sweden (Ebert et al., 2012) and the MDV (Schiller et al., 2009), though higher than those measured from other high
283 elevation, inland locations in Victoria Land (Dickinson et al., 2012; Valletta et al., 2015). Our inventory from
284 Roberts Massif is the same as the inventory reported for a nearby location by Graham et al. (1997), and all of our
285 inventories are within the range of values from the Arctic (Bierman et al., 2014), despite shallower profiles.

6.1. Relationships between meteoric ^{10}Be and NO_3^- and governing processes

287 Previous studies have proposed that atmosphere-derived salt concentrations at the surface may correlate
288 with exposure ages and wetting ages in Antarctica (Everett, 1971; Graham et al., 2002, 1997; Graly et al., 2018;
289 Lyons et al., 2016; Schiller et al., 2009). Graly et al. (2018) showed that, in particular, water-soluble NO_3^- and boron
290 exhibited the strongest relationships with exposure age ($R^2 = 0.9$ and 0.99, respectively). Lyons et al. (2016) used
291 NO_3^- concentrations to estimate the amount of time since the soils were last wetted, and Graham et al. (2002)
292 attempted to calculate exposure ages using the inventory of NO_3^- in the soil. Graly et al. (2018) argue that boron is
293 the best exposure proxy due to concerns related to NO_3^- mobility under sub-arid conditions (e.g. Frey et al., 2009;
294 Michalski et al., 2005), and given that uncertainties in local accumulation rates and ion transport can result in
295 inaccurate ages when using NO_3^- alone (Graham et al., 2002; Schiller et al., 2009). Based on the results presented
296 here for hyper-arid CTAM ice-free regions and the concerns with boron mobility depending on whether the B
297 species present in the soils is BO_3^{3-} (borate) or H_3BO_3 (boric acid), we suggest that NO_3^- is suitable for interpreting
298 wetting and disturbance histories.

299 Both meteoric ^{10}Be and NO_3^- are sourced from atmospheric deposition in the Shackleton Glacier region,
300 and there appears to be a relationship between the two constituents in the soil profiles (Fig. 6b). A similar
301 relationship between soluble salts and meteoric ^{10}Be was previously documented at Roberts Massif (Graham et al.,
302 1997). NO_3^- is highly mobile in wetter systems, while ^{10}Be is less mobile under circumneutral pH. Given sustained
303 hyper-arid conditions, minimal landscape disturbance, and negligible biologic activity, one can expect meteoric ^{10}Be
304 and NO_3^- to be correlated throughout a depth profile given the similar accumulation mechanism (Everett, 1971;
305 Graham et al., 1997). Further, their inventories (Eq. 2) should increase monotonically with exposure duration.
306 Deviations from this expected relationship could be due to 1) soil wetting, either in the present or past, 2) deposition
307 of sediment with different ^{10}Be to NO_3^- ratios compared to the depositional environment, 3) changes in the flux of
308 either ^{10}Be or NO_3^- with time, and 4) additional loss of NO_3^- due to denitrification or volatilization. The latter two
309 mechanisms are likely minor processes, however, NO_3^- deposition fluxes are known to be spatially variable (Jackson

7

310 et al., 2016; Lyons et al., 1990). As described above, Roberts Massif, Bennett Platform, and Thanksgiving Valley
311 were selected for further investigation as locations which may represent different depositional environments:
312 hypothesized hyper-aridity, recent glacial activity with large moraines, and active hydrology, respectively. By
313 comparing differences in the expected and observed relationship between ^{10}Be and NO_3^-, we can infer the processes
314 which have influenced their relationship.

6.1.1. Implications for landscape disturbance and paleoclimate

316 Our work demonstrates that NO_3^- and ^{10}Be are correlated in much of the Shackleton Glacier region, and the
317 soil profiles can inform our understanding of surficial processes and soil wetting for the region. Exposure age and
318 cosmogenic nuclide data from across Antarctica show that a polar desert regime began in the mid-Miocene and has
319 persisted into modern time (Lewis et al., 2008; Marchant et al., 1996; Spector and Balco, 2020; Valletta et al., 2015).
320 Additionally, Barrett (2013) provides a detailed review of studies focused on Antarctic glacial history, particularly
321 centered around the "stabilist vs. dynamicist" debate concerning the overall stability of the EAIS. Interpreting 40+
322 years of data from published literature, they conclude that the EAIS is stable in the interior with retreat occurring
323 along the margins, including at outlet glaciers (Golledge et al., 2012). Given these findings, we would expect NO_3^-
324 and meteoric ^{10}Be concentrations to be correlated in hyper-arid Antarctic soils, such as those from the Shackleton
325 Glacier region, as both constituents are derived from atmospheric deposition with minimal alteration at the surface.
326 The major differences between the two concern transport mechanisms; meteoric ^{10}Be transport is limited by clay
327 particle mobility and NO_3^- is mobile upon soil wetting.

328 If we assume an "ideal" situation where an undisturbed hyper-arid soil has accumulated meteoric ^{10}Be (Fig.
329 3a-b), ^{10}Be concentrations would be highest at the surface and eventually decrease to background levels at depth.
330 None of the profiles we sampled and measured for meteoric ^{10}Be and NO_3^- reached background concentrations. All
331 profiles had an active layer much shallower than those from the MDV (Graham et al., 2002; Schiller et al., 2009;
332 Valletta et al., 2015). This suggests that the active layer may have deepened and shallowed throughout time, and
333 modern ^{10}Be mobility is limited to the top ~20 cm for most of the Shackleton Glacier region. Though clay particle
334 translocation by percolating water can explain the correlated behavior of ^{10}Be and NO_3^- at Roberts Massif and
335 Thanksgiving Valley, it is unlikely that the region had sufficient precipitation for significant percolation over the last
336 14 Ma, given the high NO_3^- concentrations (Menzies et al., 2006). The concentrations of fine particles in the soil
337 profiles also do not change significantly with depth, as would be expected if large precipitation or melt events were
338 frequent (Fig. 4). Additionally, the soils horizons are moderately well defined (Fig. 4), suggesting minimal
339 cryoturbation.

340 Similar to Arena Valley and Wright Valley in the MDV (Graham et al., 2002; Schiller et al., 2009), NO_3^-
341 concentrations are highest just beneath the surface at Roberts Massif, indicating shallow salt migration under an arid
342 climate. These data suggest that the samples furthest inland at Roberts Massif and Thanksgiving Valley have been
343 fairly undisturbed since at least the middle to late Pleistocene, given the estimates of exposure duration (see Section
344 6.2). Since meteoric ^{10}Be and NO_3^- at Bennett Platform are mirrored, we argue that the difference could be due to 1)
345 additional ^{10}Be delivery or 2) enhanced NO_3^- transport. Bennett Platform was the only location we sampled on a
346 large moraine (Fig. 2c), and as a constructional landform we would expect ^{10}Be to be highest at the surface and
347 decrease to background concentrations. This is generally the observed behavior. The NO_3^- profile behavior is similar
348 to those throughout the Shackleton Glacier region, though the concentrations continue to increase with depth,
349 possibly indicating some percolation of NO_3^- rich brine. What may be considered the "anomalous" data point is the
350 surface concentration of meteoric ^{10}Be. Even though we sampled a constructional landform, the sample was
351 collected between two boulder lines in a small, local depression (~1 m) (Table 2). It is probably no coincidence that
352 this location also has the greatest proportion of fine-grained material in the soil profile. The two boulder lines
353 impede wind flow and act as a sediment and snow trap, possibly resulting in a higher concentration of meteoric ^{10}Be
354 than expected simply from atmospheric deposition. The snow in the depression may also aid in NO_3^- transport when
355 melted. In this case, additional sediment-laden ^{10}Be deposition (superseding any erosion) and/or possible salt
356 transport need to be considered to accurately date the moraine.

8

6.2. Attempt at inferring surface exposure duration approximation and thoughts on glacial history

We used the relationship between the maximum meteoric [10]Be concentration in the soil profile and the meteoric [10]Be inventory (Graly et al., 2010) to speculatively infer [10]Be inventories and estimate maximum exposure durations for all eleven locations with and without erosion using Eq. 5 (Fig. 7; Table 3). As is the case for Roberts Massif and Thanksgiving Valley, the highest [10]Be concentrations may not always be at the surface for all locations; however, the relationship is sufficiently strong to provide an estimate of the [10]Be inventory and thus an exposure duration estimate.

$$t = -\frac{1}{\lambda} \cdot \ln\left[1 - \frac{\lambda I}{Q - E\rho N}\right] \tag{5}$$

We did not measure erosion rates in this study. Balter-Kennedy et al. (2020) determined that erosion rates for boulders at Roberts Massif which were less than 2 cm Ma^{-1}. Considering we are investigating soils, we chose a conservative value of 5 cm Ma^{-1} for our calculations. We chose a [10]Be flux value (Q) of 1.3 x 10^5 atoms cm^{-2} yr^{-1} from Taylor Dome (Steig et al., 1995) due to a similar climate to that of the CTAM and an absence of local meteoric [10]Be flux data.

Compared to the measured inventories from Roberts Massif, Bennett Platform, and Thanksgiving Valley (from the [10]Be depth profiles; see Section 5.1), the inferred inventories differ by ~16-130%. The inferred exposure estimates with erosion range from 58 ka to >6.5 Ma, and the estimates without erosion range from 57 ka to 1.94 Ma for Mt. Speed and Roberts Massif, respectively (Fig 8; Table 3). With the exception of Roberts Massif, Thanksgiving Valley, and Mt. Speed, the oldest surfaces are those which we sampled furthest from the glacier, which is consistent with our sampling methodology to capture younger and older soils. The sample from Roberts Massif collected closest to the glacier has an estimated exposure duration that is outside the model limits (>6.5 Ma).

The youngest surfaces we sampled from the Shackleton Glacier region are those from the lowest elevations and closest to the Ross Ice Shelf (Fig. 8). This is generally consistent with previous glacial modeling studies which show that the greatest fluctuations in glacier height during the LGM were along outlet glacier and ice shelf margins (Golledge et al., 2012; Mackintosh et al., 2011, 2014). Given the low erosion rates throughout Antarctica (Balter-Kennedy et al., 2020; Ivy-Ochs et al., 1995; Morgan et al., 2010) and possibly low background concentrations of meteoric [10]Be (Dickinson et al., 2012; Schiller et al., 2009; Valletta et al., 2015), the Mt. Speed, Mt. Wasko, and Mt. Franke samples were all likely covered by the Shackleton Glacier during the LGM, as well as the lower elevation, near-glacier samples from Mt. Heekin, Bennett Platform, and Mt. Augustana. The soils from Schroeder Hill and Roberts Massif have likely been exposed since the early Pleistocene (Fig. 8). We also attempted to estimate exposure durations using two additional methods: 1) the measured [10]Be inventories for Roberts Massif, Bennett Platform, and Thanksgiving Valley, and 2) by calculating [10]Be concentrations using regressions of NO$_3^-$ and [10]Be for all seven locations with depth profiles, as detailed in the supplementary materials. These exposure estimates are similar and range from ~100 ka at Bennet Platform to <4.5 Ma at Roberts Massif (Fig. S4; Table S3).

Sirius Group deposits were observed at Roberts Massif and were deposited as the Shackleton Glacier retreated in this region (Fig. 2a). Evidence for a dynamic EAIS is derived primarily from the diamictite rocks (tills) of the Sirius Group, which are found throughout the TAM and include well-documented outcrops in the Shackleton Glacier region, but their age is unknown (Hambrey et al., 2003). Some of the deposits contain pieces of shrubby vegetation, suggesting that the Sirius Group formed under conditions warmer than present with woody plants occupying inland portions of Antarctica (Webb et al., 1984, 1996; Webb and Harwood, 1991). Sparse marine diatoms found in the sediments were initially interpreted as evidence for the formation of the Sirius Group via glacial over riding of the TAM during the warmer Pliocene (Barrett et al., 1992), though it is now argued that the marine diatoms were wind-derived contamination, indicating that the Sirius Group is older (Scherer et al., 2016; Stroeven et al., 1996). We document a large diamictite at site RM2-8 that is underlain by soils with an inferred exposure of at least 1.9 Ma, possibly greater than 6.5 Ma. These exposure duration estimates suggest that the loose Sirius Group diamict was deposited at Roberts Massif some point after the Pliocene. While these data cannot

9

402 constrain the age of the formation, we suggest that the diamict could have formed prior to the Pliocene and was
403 transported during the Pleistocene glaciations.

404 **7. Conclusions**
405   We determined concentrations of meteoric ^{10}Be and NO_3^- in soils from eleven ice-free areas along the
406 Shackleton Glacier, Antarctica, which are among the highest measured meteoric ^{10}Be concentrations from the polar
407 regions. Concentrations of meteoric ^{10}Be spanned from 1.9 x 10^8 atoms g^{-1} at Bennett Platform to 73 x 10^8 atoms g^{-1}
408 at Roberts Massif. The concentrations of NO_3^- were similarly variable and ranged from ~1 µg g^{-1} near the ice shelf
409 to 15 mg g^{-1} near the Polar Plateau. In general, the lowest concentrations of ^{10}Be and NO_3^- we measured were at low
410 elevations, near the ice shelf, and closest to the glacier.

411   Since NO_3^- and ^{10}Be are both derived from atmospheric deposition, we expect the shape of their
412 accumulation profiles to be similar at depth in hyper-arid soils. In general, this was true for Roberts Massif and
413 Thanksgiving Valley, while NO_3^- and ^{10}Be concentrations were mirrored at Bennett Platform. We conclude that
414 much of the southern Shackleton Glacier region has maintained persistent arid conditions since at least the
415 Pleistocene, though the region may have been warmer and wetter in the past, as evidenced by the Sirius Group
416 diamict. The onset of aridity is particularly important in understanding refugia and ecological succession in TAM
417 soils. Since the parts of the region have remained hyper-arid and undisturbed for upwards of a few million years,
418 prolonged exposure has resulted in the accumulation of salts at high concentrations in the soils. It is an enigma how
419 soil organisms have persisted throughout glacial-interglacial cycles. However, it is possible that organisms have
420 survived near the glacier at locations like Mt. Augustana, where glacial advance appears to have been minimal
421 during the LGM, but seasonal summer melt has the potential to solubilize salts.

422   Overall, our data show that the relatively youngest soils we sampled were at lower elevations near the
423 Shackleton Glacier terminus and lower elevations further inland (typically near the glacier). Inferred estimates range
424 from 57 ka (though likely post LGM when corrected) to 1.94 Ma, possibly >6.5 Ma with erosion. Our sampling
425 scheme was successful in capturing a range of surface exposure durations which can contribute to growing archives
426 in the CTAM. There are outstanding issues regarding inheritance dynamics of meteoric ^{10}Be in disturbed
427 environments, and particle erosion/deposition rates, and NO_3^- mobility. We hope that future studies will further
428 evaluate the relationship between water-soluble salts (e.g., NO_3^-) and meteoric ^{10}Be as a proxies for landscape
429 disturbance and exposure age.

430

Data Availability Statement

The datasets generated for this study are included in the article or supplementary materials.

Competing Interests

The authors declare that they have no conflict of interest.

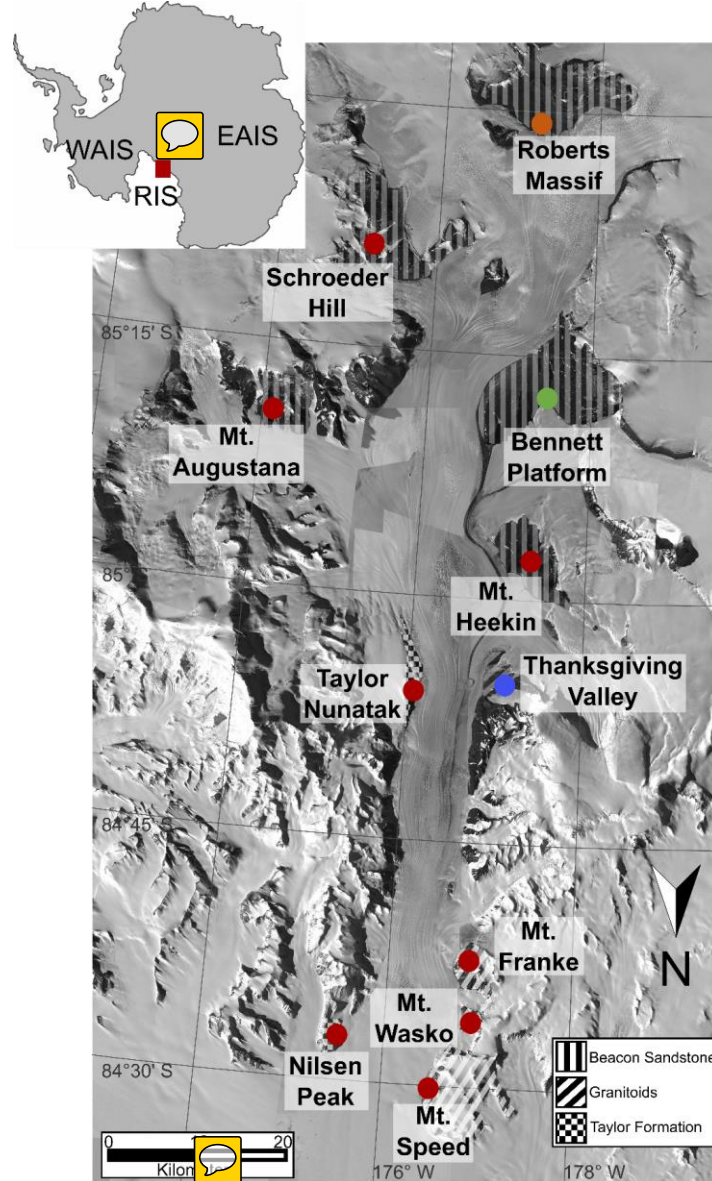**Figures:**

Figure 1: Overview map of the Shackleton Glacier region, located in the Queen Maud Mountains of the Central
Transantarctic Mountains. The red circles represent our eleven sampling locations, with an emphasis on Roberts
Massif (orange), Bennett Platform (green), and Thanksgiving Valley (blue), which have the most comprehensive
dataset in this study. The bedrock serves as primary weathering product for soil formation (Elliot and Fanning, 2008;
Paulsen et al., 2004). Base maps provided by the Polar Geospatial Center.

457

458
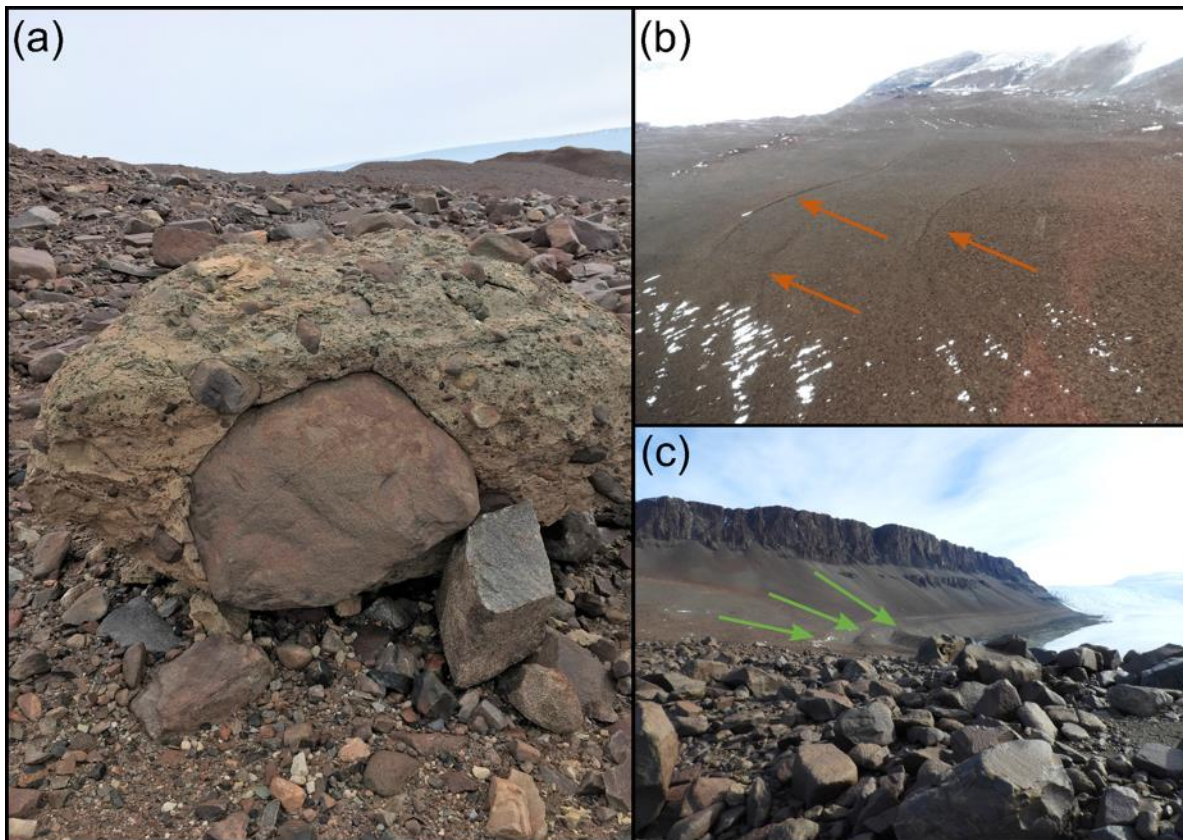
12

459

Figure 2: The Sirius Group was documented at Roberts Massif near the RM2-8 sampling location (a). Small moraines were observed at Roberts Massif (b) and large moraines at Bennett Platform (c).

462

463

464 **Figure 3:** Conceptual diagram of meteoric ^{10}Be accumulation in soils during glacial advance and retreat. In "ideal"
465 conditions, ^{10}Be accumulates in exposed soils and ^{10}Be concentrations beneath the glacier are negligible at
466 background levels (a). As the glacier retreats, ^{10}Be can begin accumulating in the recently exposed soil and an
467 inventory can be measured to calculate exposure duration. In the case where the glacier has waxed and waned
468 numerous times and the soils already contain a non-negligible "inheritance" concentration of ^{10}Be, the inventories
469 would need to be corrected for ^{10}Be inheritance (c-d) to accurately determine exposure duration.
470

471

14
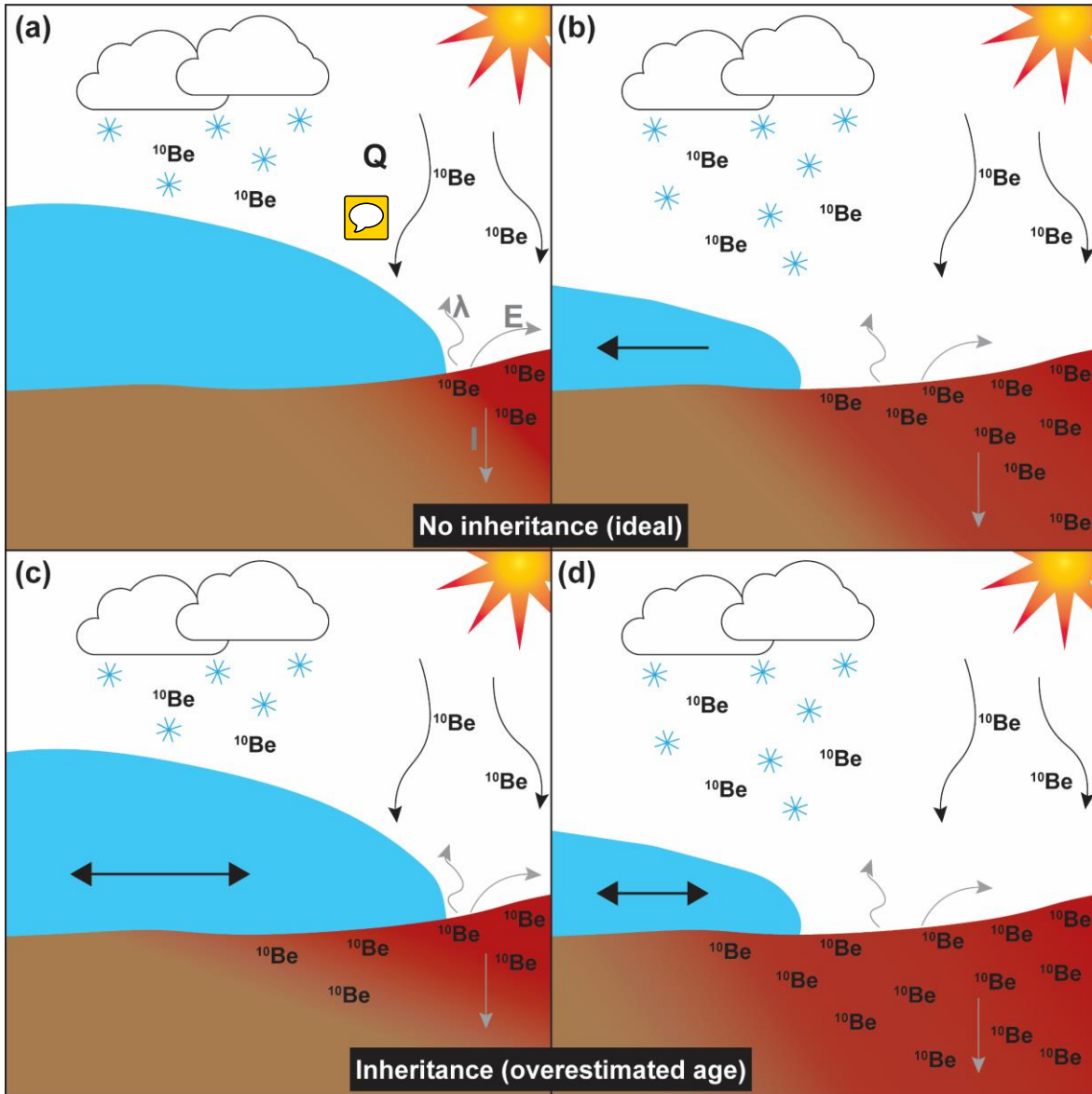
472   **Figure 4:** The grain size composition of soil profiles collected from Roberts Massif (a, orange), Bennett Platform (b,
473   green), and Thanksgiving Valley (c, blue). The soil pits from Bennett Platform and Thanksgiving Valley are also
474   shown with distinct soil horizons.
475

476
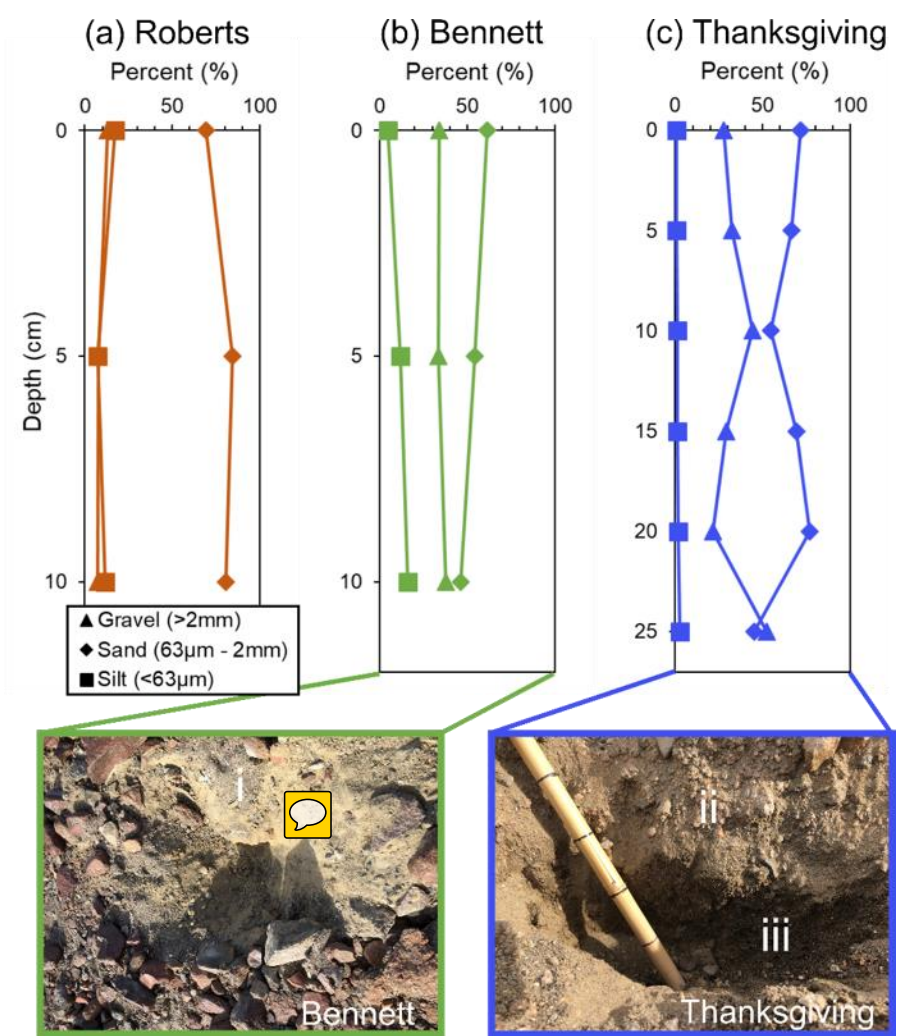
Figure 5: Spatial distribution of surface meteoric ^{10}Be concentrations in the Shackleton Glacier region (a). Where possible, two samples were collected at each location to represent surfaces closest to the glacier, which might have been glaciated during recent glacial periods, and samples furthest from the glacier that are likely to have been exposed during recent glacial periods. Insets of Roberts Massif (b), Bennett Platform (c), and Thanksgiving Valley (d) are included, as these locations ~~serve~~ have both ^{10}Be and NO_3^- depth profile data. Base maps were provided by the Polar Geospatial Center.
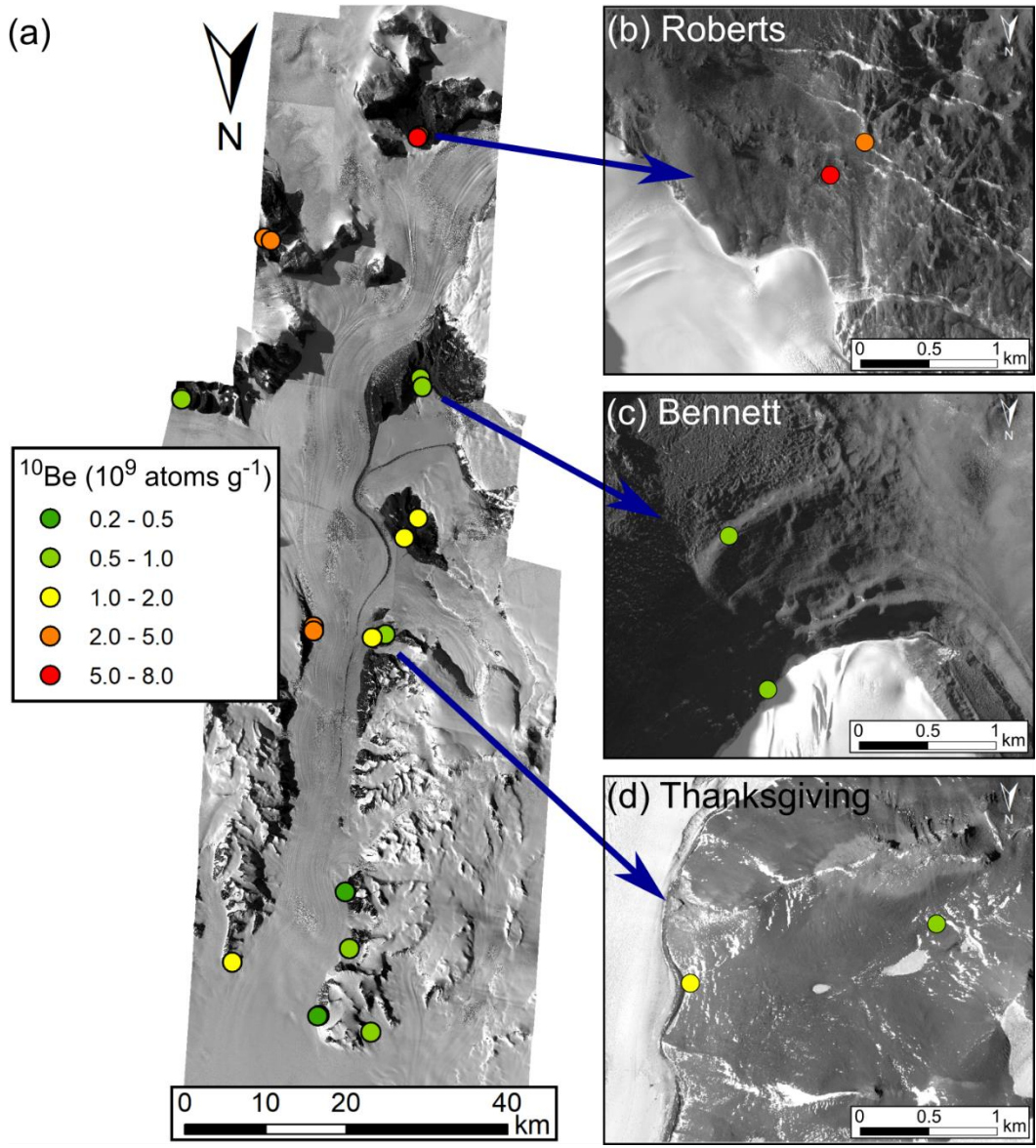
Figure 6: Soil profiles of meteoric ^{10}Be concentrations for Roberts Massif (orange), Bennett Platform (green), and Thanksgiving Valley (blue) compared to profiles from the Antarctic (Dickinson et al., 2012[*]; Schiller et al., 2009[†]; Valletta et al., 2015[‡]) and Arctic (Bierman et al., 2014[¶]; Ebert et al., 2012[§]) (a). The ^{10}Be concentration profiles were also compared to NO_3^- concentration profiles (b).
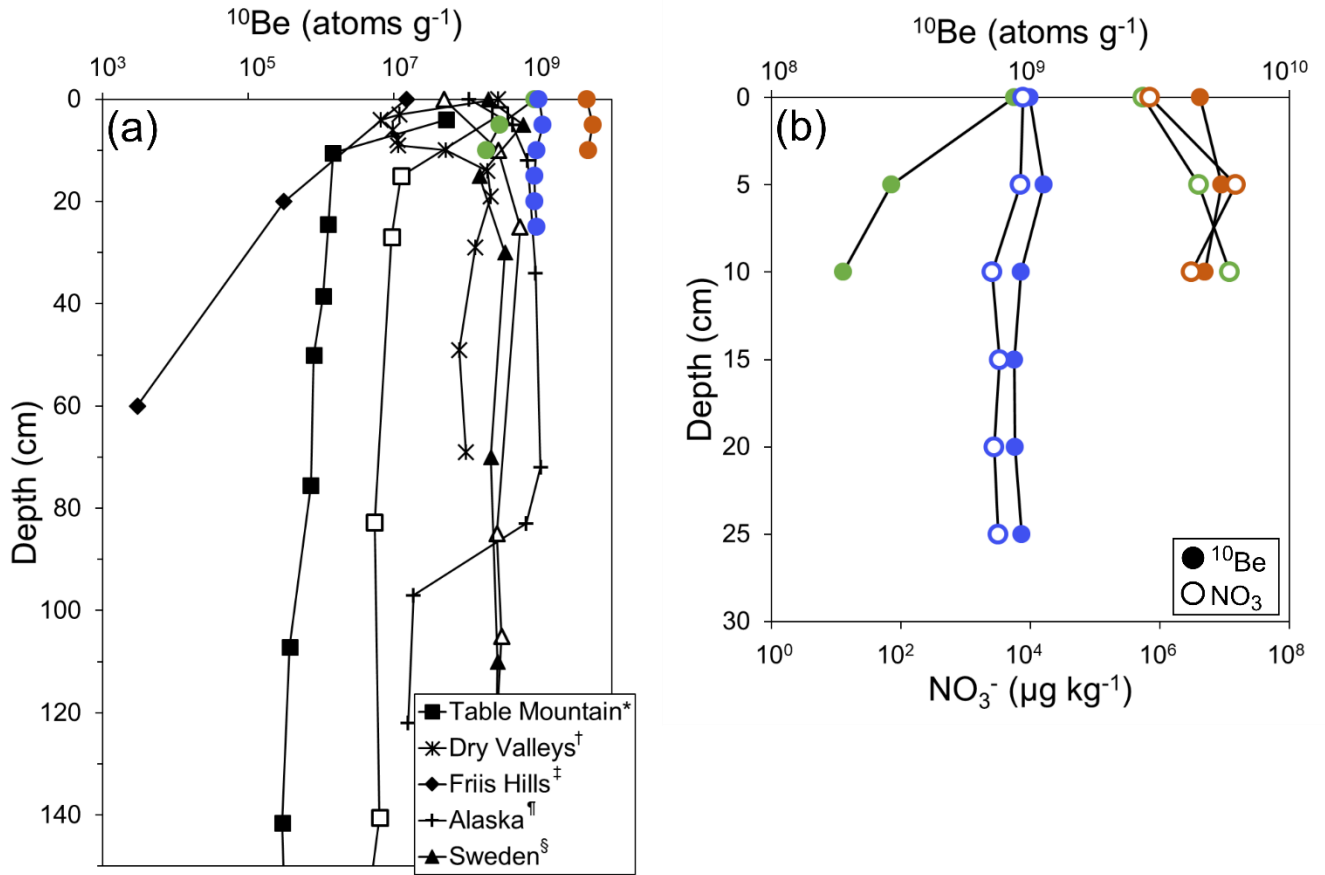
493 **Figure 7:** Relationship between the measured maximum (or surface) meteoric [10]Be concentration and the calculated
494 inventory (Eq. 2). This relationship is used to infer [10]Be inventories given a maximum or surface concentration
495 (Graly et al., 2010). The solid black line is the power relationship between concentration and inventory, while the
496 dashed grey line is the regression from Graly et al. (2010).
497
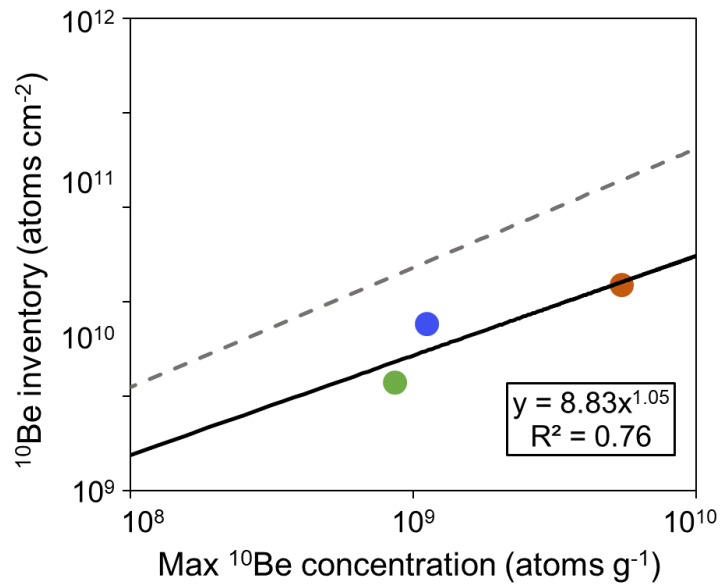
498
499

500   **Figure 8:** Inferred surface exposure durations versus distance from the coast (a) and elevation (b), with (black) and
501   without (blue) an assumed erosion term. Upward facing triangles are samples collected furthest from the glacier,
502   while downward triangles are samples collected closest to the glacier.

503
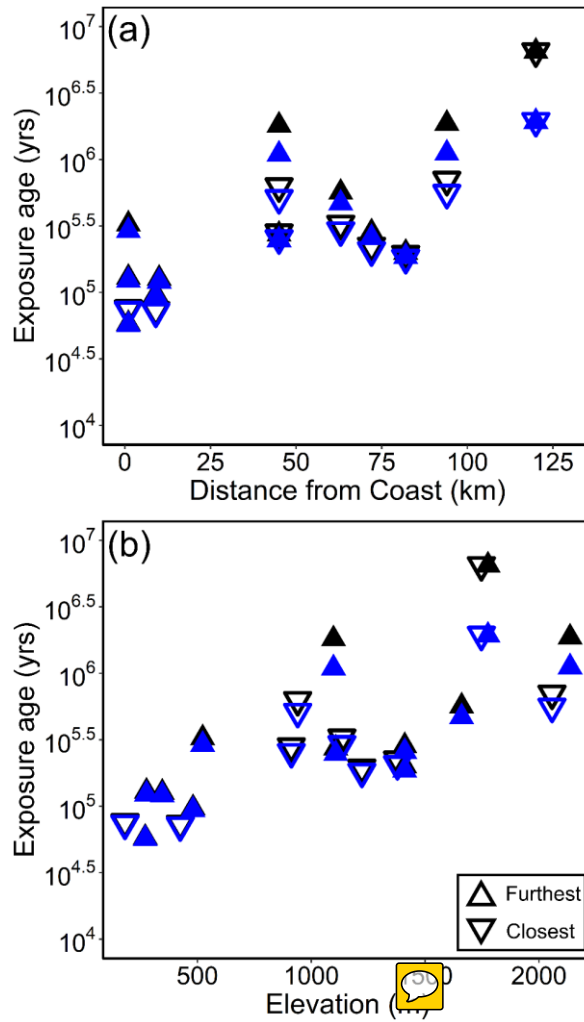
Table 1: Concentrations of meteoric ^{10}Be and water-soluble nitrate (NO$_3^-$) in Shackleton Glacier region surface soils and depth profiles. Additional information on ^{10}Be corrections is located in Table S2.

Sample Name	Location	Latitude	Longitude	Elevation (m)	Distance from Coast (km)	Depth (cm)	^{10}Be Concentration (10^9 atoms g^{-1})	NO$_3^-$ Concentration (10^5 µg kg^{-1})
AV2-1	Mt. Augustana	-85.1706	-174.1338	1410	72	0-5	1.162	7.77
AV2-1	Mt. Augustana	-85.1706	-174.1338	1410	72	5-10	-	12.2
AV2-1	Mt. Augustana	-85.1706	-174.1338	1410	72	10-15	-	13.4
AV2-8	Mt. Augustana	-85.1676	-174.1393	1378	72	0-5	0.955	-
BP2-1	Bennett Platform	-85.2121	-177.3576	1410	82	0-5	0.868	5.57
BP2-1	Bennett Platform	-85.2121	-177.3576	1410	82	5-10	0.291	39.8
BP2-1	Bennett Platform	-85.2121	-177.3576	1410	82	10-15	0.188	121
BP2-8	Bennett Platform	-85.2024	-177.3907	1222	82	0-5	0.848	-
MF2-1	Mt. Franke	-84.6236	-176.7353	480	9	0-5	0.462	0.041
MF2-1	Mt. Franke	-84.6236	-176.7353	480	9	5-10	-	0.014
MF2-1	Mt. Franke	-84.6236	-176.7353	480	9	10-15	-	0.010
MF2-1	Mt. Franke	-84.6236	-176.7353	480	9	15-20	-	0.011
MF2-4	Mt. Franke	-84.6237	-176.7252	424	9	0-5	0.360	-
MH2-1	Mt. Heekin	-85.0299	-177.2405	1098	63	0-5	1.956	18.0
MH2-1	Mt. Heekin	-85.0299	-177.2405	1098	63	5-10	-	27.4
MH2-1	Mt. Heekin	-85.0299	-177.2405	1098	63	10-15	-	18.8
MH2-8	Mt. Heekin	-85.0528	-177.4099	1209	63	0-5	1.300	-
MSP2-1	Mt. Speed	-84.4819	-176.5070	270	0	0-5	0.291	-
MSP2-4	Mt. Speed	-84.4811	-176.4864	181	0	0-5	0.370	-
MSP4-1	Mt. Speed	-84.4661	-177.1224	276	0	0-5	0.596	-
MW4-1	Mt. Wasko	-84.5600	-176.8177	345	10	0-5	0.586	-
NP2-5	Nilsen Peak	-84.6227	-176.7501	522	0	0-5	1.295	-
RM2-1	Roberts Massif	-85.4879	-177.1844	1776	120	0-5	4.538	6.94
RM2-1	Roberts Massif	-85.4879	-177.1844	1776	120	5-10	5.475	149
RM2-1	Roberts Massif	-85.4879	-177.1844	1776	120	10-15	4.721	30.7
RM2-8	Roberts Massif	-85.4857	-177.1549	1747	120	0-5	7.327	-
SH3-2	Schroeder Hill	-85.3597	-175.0693	2137	94	0-5	3.850	75.5
SH3-2	Schroeder Hill	-85.3597	-175.0693	2137	94	5-10	-	16.1

SH3-2	Schroeder Hill	-85.3597	-175.0693	2137	94	10-15	-	41.6
SH3-8	Schroeder Hill	-85.3569	-175.1621	2057	94	0-5	2.267	-
TGV2-1	Thanksgiving Valley	-84.9190	-177.0603	1107	45	0-5	0.993	0.077
TGV2-1	Thanksgiving Valley	-84.9190	-177.0603	1107	45	5-10	1.125	0.071
TGV2-1	Thanksgiving Valley	-84.9190	-177.0603	1107	45	10-15	0.921	0.025
TGV2-1	Thanksgiving Valley	-84.9190	-177.0603	1107	45	15-20	0.864	0.033
TGV2-1	Thanksgiving Valley	-84.9190	-177.0603	1107	45	20-25	0.874	0.028
TGV2-1	Thanksgiving Valley	-84.9190	-177.0603	1107	45	25-30	0.925	0.031
TGV2-8	Thanksgiving Valley	-84.9145	-176.8860	912	45	0-5	1.152	-
TN3-1	Taylor Nunatak	-84.9227	-176.1242	1097	45	0-5	3.802	-
TN3-5	Taylor Nunatak	-84.9182	-176.1282	940	45	0-5	2.105	

507

508 **Table 2:** Surface features of the sample locations from the Shackleton Glacier region.
509

Location	Sample name	Sample description
Mt. Augustana	AV2-1	Up valley from Gallup Glacier (tributary glacier); at valley floor; surface covered by cobbles and pebbles; red-stained sandstones nearby; frozen ground at bottom of depth profile
Mt. Augustana	AV2-8	At toe of Gallup Glacier; surface covered primarily by boulders; mainly sand between boulders
Bennett Platform	BP2-1	On larger moraine; local depression between two boulder lines, up valley from McGregor Glacier (tributary glacier); at valley floor
Bennett Platform	BP2-8	At toe of McGregor Glacier (tributary glacier); surface covered primarily by boulders; mainly sand between boulders
Mt. Franke	MF2-1	Bottom of wide valley floor; near small moraine; frozen soil at bottom of depth profile
Mt. Franke	MF2-4	Bottom of wide valley floor; near small moraine
Mt. Heekin	MH2-1	On high-elevation saddle; surface covered by sparse small boulders, cobbles, and pebbles; poorly consolidated till; frozen ground at bottom of profile
Mt. Heekin	MH2-8	At toe of Baldwin Glacier (alpine glacier) on valley floor; two ponds nearby; surface covered by loose rocks and sand; poorly consolidated till; possible polygonal surface nearby
Mt. Speed	MSP2-1	Steep slope; large granite boulders; scree
Mt. Speed	MSP2-4	Near cliff by Shackleton Glacier; large granite boulders; scree
Mt. Speed	MSP4-1	Spur on level with glacier; frozen soil near 5 cm depth
Mt. Wasko	MW4-1	Steep slope; large granite boulders; scree; nearby snowpack
Nilsen Peak	NP2-5	On ridge; near large snow patch
Roberts Massif	RM2-1	Near thin moraine; red-stained sandstones nearby with etches; frozen ground at bottom of depth profile
Roberts Massif	RM2-8	Near thin moraine and Sirius Group diamict; large boulders nearby with unconsolidated sediment
Schroeder Hill	SH3-2	Red-stained sandstone; poorly consolidated till; bedrock at bottom of profile
Schroeder Hill	SH3-8	Red-stained sandstone; poorly consolidated till;
Thanksgiving Valley	TGV2-1	Lightly uphill on valley wall; poorly consolidated till; frozen ground at bottom of depth profile; polygonal surface nearby
Thanksgiving Valley	TGV2-8	At the toe of Shackleton Glacier; near thin moraines, surface covered primarily large boulders
Taylor Nunatak	TN3-1	On ridge; surface covered by small boulders with underlaying silt; frozen ground at bottom of depth profile
Taylor Nunatak	TN3-5	Valley floor; nearby snow patches; few glacial erratics; surface covered primarily by small boulders and cobbles with underlaying silt

510

511

512

513 **Table 3:** Estimated exposure durations using relationship between maximum ^{10}Be concentration and inventory in
514 Figure 7 (Graly et al., 2010).
515

Sample name	Measured inventory (10^{11} atoms)	Inferred inventory (10^{11} atoms)	Inferred exposure duration with E (Ma)	Inferred exposure duration without E (Ma)
AV2-1		0.38	0.285	0.258
AV2-8		0.33	0.224	0.207
BP2-1	0.135	0.31	0.200	0.186
BP2-8		0.31	0.195	0.181
MF2-1		0.21	0.097	0.094
MF2-4		0.18	0.074	0.072
MH2-1		0.59	0.565	0.469
MH2-8		0.42	0.328	0.292
MSP2-1		0.16	0.058	0.057
MSP2-4		0.18	0.076	0.074
MSP4-1		0.24	0.129	0.123
MW4-1		0.24	0.127	0.121
NP2-5		0.42	0.326	0.291
RM2-1	1.47	1.24	>6.5*	1.93
RM2-8		1.50	>6.5*	1.94
SH3-2		1.07	1.87	1.11
SH3-8		0.67	0.702	0.560
TGV2-1	0.535	0.34	0.274	0.248
TGV2-8		0.38	0.282	0.255
TN3-1		1.06	1.81	1.09
TN3-5		0.62	0.628	0.512
*Outside of model range				

516

517

518 **References**

519 Ackert, R. P. and Kurz, M. D.: Age and uplift rates of Sirius Group sediments in the Dominion Range, Antarctica,
520 from surface exposure dating and geomorphology, Glob. Planet. Change, 42(1–4), 207–225,
521 doi:10.1016/j.gloplacha.2004.02.001, 2004.

522 Anderson, J. B., Shipp, S. S., Lowe, A. L., Wellner, J. S. and Mosola, A. B.: The Antarctic Ice Sheet during the Last
523 Glacial Maximum and its subsequent retreat history: a review, Quat. Sci. Rev., 21, 49–70, doi:10.1016/S0277-
524 3791(01)00083-X, 2002.

525 Augustin, L., Barbante, C., Barnes, P. R. F., Barnola, J. M., Bigler, M., Castellano, E., Cattani, O., Chappellaz, J.,
526 Dahl-Jensen, D., Delmonte, B., Dreyfus, G., Durand, G., Falourd, S., Fischer, H., Flückiger, J., Hansson, M. E.,
527 Huybrechts, P., Jugie, G., Johnsen, S. J., Jouzel, J., Kaufmann, P., Kipfstuhl, J., Lambert, F., Lipenkov, V. Y., Littot,
528 G. C., Longinelli, A., Lorrain, R., Maggi, V., Masson-Delmotte, V., Miller, H., Mulvaney, R., Oerlemans, J., Oerter,
529 H., Orombelli, G., Parrenin, F., Peel, D. A., Petit, J. R., Raynaud, D., Ritz, C., Ruth, U., Schwander, J., Siegenthaler,
530 U., Souchez, R., Stauffer, B., Steffensen, J. P., Stenni, B., Stocker, T. F., Tabacco, I. E., Udisti, R., van de Wal, R. S.
531 W., van den Broeke, M., Weiss, J., Wilhelms, F., Winther, J. G., Wolff, E. W. and Zucchelli, M.: Eight glacial
532 cycles from an Antarctic ice core, Nature, 429(6992), 623–628, doi:10.1038/nature02599, 2004.

533 Balter-Kennedy, A., Bromley, G., Balco, G., Thomas, H. and Jackson, M. S.: A 14.5-million-year record of East
534 Antarctic Ice Sheet fluctuations from the central Transantarctic Mountains, constrained with cosmogenic 3He, 10Be,
535 21Ne, and 26Al, Cryosph., 14(8), 2647–2672, doi:10.5194/tc-2020-57, 2020.

536 Barrett, P. J., Adams, C. J., McIntosh, W. C., Swisher, C. C. and Wilson, G. S.: Geochronological evidence
537 supporting Antarctic deglaciation three million years ago, Nature, 359, 816–818, 1992.

538 Bierman, P. R., Corbett, L. B., Graly, J. A., Neumann, T. A., Lini, A., Crosby, B. T. and Rood, D. H.: Preservation
539 of a Preglacial Landscape Under the Center of the Greenland Ice Sheet, Science (80-.)., 344, 402–405,
540 doi:10.4159/harvard.9780674430501.c21, 2014.

541 Bockheim, J. G.: Landform and Soil Development in the McMurdo Dry Valleys, Antarctica: A Regional Synthesis,
542 Arctic, Antarct. Alp. Res., 34(3), 308–317, doi:10.1080/15230430.2002.12003499, 2002.

543 Bromley, G. R. M., Hall, B. L., Stone, J. O., Conway, H. and Todd, C. E.: Late Cenozoic deposits at Reedy Glacier,
544 Transantarctic Mountains: implications for former thickness of the West Antarctic Ice Sheet, Quat. Sci. Rev., 29(3–
545 4), 384–398, doi:10.1016/j.quascirev.2009.07.001, 2010.

546 Brown, E. T., Edmond, J. M., Raisbeck, G. M., Bourlès, D. L., Yiou, F. and Measures, C. I.: Beryllium isotope
547 geochemistry in tropical river basins, Geochim. Cosmochim. Acta, 56(4), 1607–1624, doi:10.1016/0016-
548 7037(92)90228-B, 1992.

549 Cary, S. C., McDonald, I. R., Barrett, J. E. and Cowan, D. A.: On the rocks: The microbiology of Antarctic Dry
550 Valley soils, Nat. Rev. Microbiol., 8(2), 129–138, doi:10.1038/nrmicro2281, 2010.

551 Claridge, G. G. C. and Campbell, I. B.: Origin of nitrate deposits., 1968a.

552 Claridge, G. G. C. and Campbell, I. B.: Soils of the Shackleton glacier region, Queen Maud Range, Antarctica, New
553 Zeal. J. Sci., 11(2), 171–218, 1968b.

554 Claridge, G. G. C. and Campbell, I. B.: Salts in Antarctic soils, their distribution and relationship to soil processes,
555 Soil Sci., 123(6), 377–384, 1977.

556 Clark, P. U., Dyke, A. S., Shakun, J. D., Carlson, A. E., Clark, J., Wohlfarth, B., Mitrovica, J. X., Hostetler, S. W.
557 and McCabe, A. M.: The Last Glacial Maximum, Science (80-.)., 325, 710–714, doi:10.1126/science.1172873,
558 2009.

559 Collins, G. E., Hogg, I. D., Convey, P., Sancho, L. G., Cowan, D. A., Lyons, W. B., Adams, B. J., Wall, D. H. and
560 Green, T. G. A.: Genetic diversity of soil invertebrates corroborates timing estimates for past collapses of the West
561 Antarctic Ice Sheet, Proc. Natl. Acad. Sci. U. S. A., 117(36), 22293–22302, doi:10.1073/pnas.2007925117, 2020.

562 Convey, P., Gibson, J. A. E., Hillenbrand, C. D., Hodgson, D. A., Pugh, P. J. A., Smellie, J. L. and Stevens, M. I.:

Antarctic terrestrial life - Challenging the history of the frozen continent?, Biol. Rev., 83(2), 103–117, doi:10.1111/j.1469-185X.2008.00034.x, 2008.

Diaz, M. A., Li, J., Michalski, G., Darrah, T. H., Adams, B. J., Wall, D. H., Hogg, I. D., Fierer, N., Welch, S. A., Gardner, C. B. and Lyons, W. B.: Stable isotopes of nitrate, sulfate, and carbonate in soils from the Transantarctic Mountains, Antarctica: A record of atmospheric deposition and chemical weathering, Front. Earth Sci., 8(341), doi:10.3389/feart.2020.00341, 2020.

Dickinson, W. W., Schiller, M., Ditchburn, B. G., Graham, I. J. and Zondervan, A.: Meteoric Be-10 from Sirius Group suggests high elevation McMurdo Dry Valleys permanently frozen since 6 Ma, Earth Planet. Sci. Lett., 355–356, 13–19, doi:10.1016/j.epsl.2012.09.003, 2012.

Ebert, K., Willenbring, J., Norton, K. P., Hall, A. and Hättestrand, C.: Meteoric 10Be concentrations from saprolite and till in northern Sweden: Implications for glacial erosion and age, Quat. Geochronol., 12, 11–22, doi:10.1016/j.quageo.2012.05.005, 2012.

Elliot, D. H. and Fanning, C. M.: Detrital zircons from upper Permian and lower Triassic Victoria Group sandstones, Shackleton Glacier region, Antarctica: Evidence for multiple sources along the Gondwana plate margin, Gondwana Res., 13, 259–274, doi:10.1016/j.gr.2007.05.003, 2008.

Elliot, D. H., Collinson, J. W. and Green, W. J.: Lakes in dry valleys at 85°S near Mount Heekin, Shackleton Glacier, Antarct. J. United States, 31(2), 25–27, 1996.

Everett, K. R.: SOILS OF THE MESERVE GLACIER AREA, WRIGHT VALLEY, SOUTH VICTORIA LAND, ANTARCTICA, Soil Sci., 112(6), 425–438 [online] Available from: https://oce.ovid.com/article/00010694-197112000-00007/HTML (Accessed 17 June 2021), 1971.

Fraser, C. I., Nikula, R., Ruzzante, D. E. and Waters, J. M.: Poleward bound: Biological impacts of Southern Hemisphere glaciation, Trends Ecol. Evol., 27(8), 462–471, doi:10.1016/j.tree.2012.04.011, 2012.

Frey, M. M., Savarino, J., Morin, S., Erbland, J. and Martins, J. M. F.: Photolysis imprint in the nitrate stable isotope signal in snow and atmosphere of East Antarctica and implications for reactive nitrogen cycling., 2009.

Gasson, E., DeConto, R. M., Pollard, D. and Levy, R. H.: Dynamic Antarctic ice sheet during the early to mid-Miocene, Proc. Natl. Acad. Sci. U. S. A., 113(13), 3459–3464, doi:10.1073/pnas.1516130113, 2016.

Golledge, N. R., Fogwill, C. J., Mackintosh, A. N. and Buckley, K. M.: Dynamics of the last glacial maximum Antarctic ice-sheet and its response to ocean forcing, Proc. Natl. Acad. Sci. U. S. A., 109(40), 16052–16056, doi:10.1073/pnas.1205385109, 2012.

Golledge, N. R., Levy, R. H., McKay, R. M., Fogwill, C. J., White, D. A., Graham, A. G. C., Smith, J. A., Hillenbrand, C. D., Licht, K. J., Denton, G. H., Ackert, R. P., Maas, S. M. and Hall, B. L.: Glaciology and geological signature of the Last Glacial Maximum Antarctic ice sheet, Quat. Sci. Rev., 78, 225–247, doi:10.1016/j.quascirev.2013.08.011, 2013.

Graham, I., Ditchburn, R. G., Claridge, G. G. G., Whitehead, N. E., Zondervan, A. and Sheppard, D. S.: Dating Antarctic soils using atmospheric derived 10Be and nitrate, R. Soc. New Zeal. Bull., 35, 429–436, 2002.

Graham, I. J., Ditchbum, R. G., Sparks, R. J. and Whitehead, N. E.: 10Be investigations of sediments, soils and loess at GNS, Nucl. Instruments Methods Phys. Res. B, 123, 307–318, 1997.

Graly, J. A., Bierman, P. R., Reusser, L. J. and Pavich, M. J.: Meteoric 10Be in soil profiles - A global meta-analysis, Geochim. Cosmochim. Acta, 74, 6814–6829, doi:10.1016/j.gca.2010.08.036, 2010.

Graly, J. A., Licht, K. J., Druschel, G. K. and Kaplan, M. R.: Polar desert chronologies through quantitative measurements of salt accumulation, Geology, 46(4), 351–354, doi:10.1130/G39650.1, 2018.

Gulick, S. P. S., Shevenell, A. E., Montelli, A., Fernandez, R., Smith, C., Warny, S., Bohaty, S. M., Sjunneskog, C., Leventer, A., Frederick, B. and Blankenship, D. D.: Initiation and long-term instability of the East Antarctic Ice Sheet, Nature, 552(7684), 225–229, doi:10.1038/nature25026, 2017.

607 Hambrey, M. J., Webb, P. N., Harwood, D. M. and Krissek, L. A.: Neogene glacial record from the Sirius Group of
608 the Shackleton Glacier region, central Transantarctic Mountains, Antarctica, GSA Bull., 115(8), 994–1015,
609 doi:10.1130/B25183.1, 2003.

610 Ivy-Ochs, S., Schluchter, C., Kubik, P. W., Dittrich-Hannen, B. and Beer, J.: Minimum 10Be exposure ages of early
611 Pliocene for the Table Mountain plateau and the Sirius Group at Mount Fleming, Dry Valleys, Antarctica, Geology,
612 23(11), 1007–1010, 1995.

613 Jackson, A., Davila, A. F., Böhlke, J. K., Sturchio, N. C., Sevanthi, R., Estrada, N., Brundrett, M., Lacelle, D.,
614 McKay, C. P., Poghosyan, A., Pollard, W. and Zacny, K.: Deposition, accumulation, and alteration of Cl-, NO3-,
615 ClO4- and ClO3- salts in a hyper-arid polar environment: Mass balance and isotopic constraints, Geochim.
616 Cosmochim. Acta, 182, 197–215, doi:10.1016/j.gca.2016.03.012, 2016.

617 Jones, R. S., Mackintosh, A. N., Norton, K. P., Golledge, N. R., Fogwill, C. J., Kubik, P. W., Christl, M. and
618 Greenwood, S. L.: Rapid Holocene thinning of an East Antarctic outlet glacier driven by marine ice sheet instability,
619 Nat. Commun., 6(8910), 9910, doi:10.1038/ncomms9910, 2015.

620 Kaplan, M. R., Licht, K. J., Winckler, G., Schaefer, J. M., Bader, N., Mathieson, C., Roberts, M., Kassab, C. M.,
621 Schwartz, R. and Graly, J. A.: Middle to Late Pleistocene stability of the central East Antarctic Ice Sheet at the head
622 of Law Glacier, Geology, 45(11), 963–966, doi:10.1130/G39189.1, 2017.

623 Korschinek, G., Bergmaier, A., Faestermann, T., Gerstmann, U. C., Knie, K., Rugel, G., Wallner, A., Dillmann, I.,
624 Dollinger, G., von Gostomski, C. L., Kossert, K., Maiti, M., Poutivtsev, M. and Remmert, A.: A new value for the
625 half-life of 10Be by Heavy-Ion Elastic Recoil Detection and liquid scintillation counting, Nucl. Instruments
626 Methods Phys. Res. Sect. B Beam Interact. with Mater. Atoms, 268(2), 187–191, doi:10.1016/j.nimb.2009.09.020,
627 2010.

628 Lewis, A. R., Marchant, D. R., Ashworth, A. C., Hedenäs, L., Hemming, S. R., Johnson, J. V., Leng, M. J.,
629 Machlus, M. L., Newton, A. E., Raine, J. I., Willenbring, J. K., Williams, M. and Wolfe, A. P.: Mid-Miocene
630 cooling and the extinction of tundra in continental Antarctica, Proc. Natl. Acad. Sci. U. S. A., 105(31), 10676–
631 10680, doi:10.1073/pnas.0802501105, 2008.

632 Lyons, W. B., Mayewski, P. A., Spencer, M. J. and Twickler, M. S.: Nitrate concentrations in snow from remote
633 areas: implication for the global NOx flux, Biogeochemistry, 9(3), 211–222, doi:10.1007/BF00000599, 1990.

634 Lyons, W. B., Deuerling, K., Welch, K. A., Welch, S. A., Michalski, G., Walters, W. W., Nielsen, U., Wall, D. H.,
635 Hogg, I. and Adams, B. J.: The Soil Geochemistry in the Beardmore Glacier Region, Antarctica: Implications for
636 Terrestrial Ecosystem History, Sci. Rep., 6, 26189, doi:10.1038/srep26189, 2016.

637 Mackintosh, A., Golledge, N., Domack, E., Dunbar, R., Leventer, A., White, D., Pollard, D., Deconto, R., Fink, D.,
638 Zwartz, D., Gore, D. and Lavoie, C.: Retreat of the East Antarctic ice sheet during the last glacial termination, Nat.
639 Geosci., 4(3), 195–202, doi:10.1038/ngeo1061, 2011.

640 Mackintosh, A. N., Verleyen, E., O'Brien, P. E., White, D. A., Jones, R. S., McKay, R., Dunbar, R., Gore, D. B.,
641 Fink, D., Post, A. L., Miura, H., Leventer, A., Goodwin, I., Hodgson, D. A., Lilly, K., Crosta, X., Golledge, N. R.,
642 Wagner, B., Berg, S., van Ommen, T., Zwartz, D., Roberts, S. J., Vyverman, W. and Masse, G.: Retreat history of
643 the East Antarctic Ice Sheet since the Last Glacial Maximum, Quat. Sci. Rev., 100, 10–30,
644 doi:10.1016/j.quascirev.2013.07.024, 2014.

645 Marchant, D. R., Denton, G. H., Swisher, C. C. and Potter, N.: Late Cenozoic Antarctic paleoclimate reconstructed
646 from volcanic ashes in the Dry Valleys region of southern Victoria Land, Geol. Soc. Am. Bull., 108(2), 181–194,
647 doi:https://doi.org/10.1130/0016-7606(1996)108%3C0181:LCAPRF%3E2.3.CO;2, 1996.

648 McHargue, L. R. and Damon, P. E.: The global beryllium 10 cycle, Rev. Geophys., 29(2), 141–158,
649 doi:10.1029/91RG00072, 1991.

650 Menzies, J., van der Meer, J. J. M. and Rose, J.: Till-as a glacial "tectomict", its internal architecture, and the
651 development of a "typing" method for till differentiation, Geomorphology, 75, 172–200,
652 doi:10.1016/j.geomorph.2004.02.017, 2006.

653 Michalski, G., Bockheim, J. G., Kendall, C. and Thiemens, M.: Isotopic composition of Antarctic Dry Valley
654 nitrate: Implications for NOy sources and cycling in Antarctica, Geophys. Res. Lett., 32(13), 1–4,
655 doi:10.1029/2004GL022121, 2005.

656 Morgan, D., Putkonen, J., Balco, G. and Stone, J.: Quantifying regolith erosion rates with cosmogenic nuclides 10
657 Be and 26 Al in the McMurdo Dry Valleys, Antarctica, J. Geophys. Res., 115, F03037, doi:10.1029/2009JF001443,
658 2010.

659 Nishiizumi, K., Imamura, M., Caffee, M. W., Southon, J. R., Finkel, R. C. and McAninch, J.: Absolute calibration of
660 10Be AMS standards, Nucl. Instruments Methods Phys. Res. B, 258, 403–413, doi:10.1016/j.nimb.2007.01.297,
661 2007.

662 Paulsen, T. S., Encarnación, J. and Grunow, A. M.: Structure and timing of transpressional deformation in the
663 Shackleton Glacier area, Ross orogen, Antarctica, J. Geol. Soc. London., 161(6), 1027–1038, doi:10.1144/0016-
664 764903-040, 2004.

665 Pavich, M. J., Brown, L., Klein, J. and Middleton, R.: 10Be accumulation in a soil chronosequence, Earth Planet.
666 Sci. Lett., 68, 198–204, doi:10.1016/0012-821X(84)90151-1, 1984.

667 Pavich, M. J., Brown, L., Harden, J., Klein, J. and Middleton, R.: 10Be distribution in soils from Merced River
668 terraces, California, Geochim. Cosmochim. Acta, 50, 1727–1735, doi:10.1016/0016-7037(86)90134-1, 1986.

669 Pollard, D. and DeConto, R. M.: Modelling West Antarctic ice sheet growth and collapse through the past five
670 million years, Nature, 458(7236), 329–332, doi:10.1038/nature07809, 2009.

671 Reich, M. and Bao, H.: Nitrate deposits of the Atacama Desert: A marker of long-term hyperaridity, Elements,
672 14(4), 251–256, doi:10.2138/gselements.14.4.251, 2018.

673 Scarrow, J. W., Balks, M. R. and Almond, P. C.: Three soil chronosequences in recessional glacial deposits near the
674 polar plateau, in the Central Transantarctic Mountains, Antarctica, Antarct. Sci., 26(5), 573–583,
675 doi:10.1017/S0954102014000078, 2014.

676 Scherer, R. P., DeConto, R. M., Pollard, D. and Alley, R. B.: Windblown Pliocene diatoms and East Antarctic Ice
677 Sheet retreat, Nat. Commun., 7(1), 1–9, doi:10.1038/ncomms12957, 2016.

678 Schiller, M., Dickinson, W., Ditchburn, R. G., Graham, I. J. and Zondervan, A.: Atmospheric 10 Be in an Antarctic
679 soil: Implications for climate change, J. Geophys. Res., 114(F1), 1–8, doi:10.1029/2008jf001052, 2009.

680 Spector, P. and Balco, G.: Exposure-age data from across Antarctica reveal mid-Miocene establishment of polar
681 desert climate, Geol. Soc. Am. | Geol., 1, doi:10.1130/G47783.1, 2020.

682 Spector, P., Stone, J., Cowdery, S. G., Hall, B., Conway, H. and Bromley, G.: Rapid early-Holocene deglaciation in
683 the Ross Sea, Antarctica, Geophys. Res. Lett., 44(15), 7817–7825, doi:10.1002/2017GL074216, 2017.

684 Steig, E., Stuiver, M. and Polissar, P.: Cosmogenic isotope concentrations at Taylor Dome, Antarctica, Antarct. J.
685 United States, 30, 95–97, 1995.

686 Stevens, M. I. and Hogg, I. D.: Long-term isolation and recent range expansion from glacial refugia revealed for the
687 endemic springtail Gomphiocephalus hodgsoni from Victoria Land, Antarctica, Mol. Ecol., 12(9), 2357–2369,
688 doi:10.1046/j.1365-294X.2003.01907.x, 2003.

689 Stone, J.: A rapid fusion method for separation of beryllium-10 from soils and silicates, Geochim. Cosmochim.
690 Acta, 62(3), 555–561, doi:10.1016/S0016-7037(97)00340-2, 1998.

691 Stroeven, A. P., Prentice, M. L. and Kleman, J.: On marine microfossil transport and pathways in Antarctica during
692 the late Neogene: Evidence from the Sirius Group at Mount Fleming, Geology, 24(8), 727–730, doi:10.1130/0091-
693 7613(1996)024<0727:ommtap>2.3.co;2, 1996.

694 Talarico, F. M., McKay, R. M., Powell, R. D., Sandroni, S. and Naish, T.: Late Cenozoic oscillations of Antarctic
695 ice sheets revealed by provenance of basement clasts and grain detrital modes in ANDRILL core AND-1B, Glob.
696 Planet. Change, 96–97, 23–40, doi:10.1016/j.gloplacha.2009.12.002, 2012.

697   Valletta, R. D., Willenbring, J. K., Lewis, A. R., Ashworth, A. C. and Caffee, M.: Extreme decay of meteoric
698   beryllium-10 as a proxy for persistent aridity, Sci. Rep., 5, 17813, doi:10.1038/srep17813, 2015.

699   Webb, P. N. and Harwood, D. M.: Late Cenozoic glacial history of the Ross embayment, Antarctica, Quat. Sci.
700   Rev., 10(2–3), 215–223, doi:10.1016/0277-3791(91)90020-U, 1991.

701   Webb, P. N., Harwood, D. M., McKelvey, B. C., Mercer, J. H. and Stott, L. D.: Cenozoic marine sedimentation and
702   ice-volume variation on the East Antarctic craton, Geology, 12(5), 287–291, doi:10.1130/0091-
703   7613(1984)12<287:cmsaiv>2.0.co;2, 1984.

704   Webb, P. N., Harwood, D. M., Mabin, M. G. C. and McKelvey, B. C.: A marine and terrestrial Sirius Group
705   succession, middle Beardmore Glacier-Queen Alexandra Range, Transantarctic Mountains, Antarctica, Mar.
706   Micropaleontol., 27(1–4), 273–297, doi:10.1016/0377-8398(95)00066-6, 1996.

707   Welch, K. A., Lyons, W. B., Whisner, C., Gardner, C. B., Gooseff, M. N., Mcknight, D. M. and Priscu, J. C.: Spatial
708   variations in the geochemistry of glacial meltwater streams in the Taylor Valley, Antarctica, Antarct. Sci., 22(6),
709   662–672, doi:10.1017/S0954102010000702, 2010.

710   Willenbring, J. K. and von Blanckenburg, F.: Meteoric cosmogenic Beryllium-10 adsorbed to river sediment and
711   soil: Applications for Earth-surface dynamics, Earth-Science Rev., 98(1–2), 105–122,
712   doi:10.1016/j.earscirev.2009.10.008, 2010.

713   You, C. F., Lee, T. and Li, Y. H.: The partition of Be between soil and water, Chem. Geol., 77(2), 105–118,
714   doi:10.1016/0009-2541(89)90136-8, 1989.

715